Role of interfacial energy during pattern formation of electropolishing

Weidong Guo and Duane Johnson*
Department of Chemical Engineering, University of Alabama, Tuscaloosa, Alabama 35487
(Received 16 September 2002; published 18 February 2003)

This paper investigates the effect of interfacial energy on nanoscale pattern formation during electropolishing of aluminum. We correct a small error in the existing theory of Yuzhakov *et al.* that unfortunately no longer predicts stable hexagonal patterns. Upon including the interfacial energy in the derivation, the stable hexagons are recovered. We have derived the evolution equation of the aluminum interface during electropolishing and performed a linear and weakly nonlinear stability analysis. The results give values that lead to stable striped or hexagonal patterns. Results of a full nonlinear simulation of the evolution equation agree qualitatively with the weakly nonlinear results. Experimental results also verify our model, which predicts the coexistence of striped and hexagonal patterns in one sample.

DOI: 10.1103/PhysRevB.67.075411 PACS number(s): 68.03.Cd, 81.16.Rf, 82.45.Qr

I. INTRODUCTION

Porous anodized films on aluminum that produce hexagonal ordering have attracted much attention recently due to their high pore density and potential applications in the electronic and information storage industries, as well as their general use in nanotechnology.[1,2] Studies have been performed to interpret the corresponding mechanism of this structure.[3–5] The primary mechanism related to these works is field-enhanced dissolution where the electric field has an important effect on the structure of both barrier-type film (BTF) and pore-type film (PTF) domains. BTF and PTF both start from a smooth surface that will develop into pits because of electropolishing or lattice imperfections.[5] For both BTF and PTF, the Al^{3+} ion is released from the metal/oxide interface and migrates through the oxide layer, while the water splitting reaction occurs at the oxide/electrolyte interface that yields the O^{2-} ion for producing alumina.[5] The electric field enhances the dissolution and is stronger at the pore bottom where the oxide film is thinner. Therefore, a deeper pit at the metal/oxide interface is formed, and a pore is shaped.[6]

In contrast with the anodization of aluminum, another pattern technology is electropolishing, which has been extensively investigated using atomic force microscopy.[7–10] By electropolishing pure (99.99%) Al foil at various voltages in acidic electrolyte, one obtains different patterns (hexagons, stripes, or mixed patterns). Depending on the electrolyte, if the applied voltage is low, one obtains the striped pattern, while the hexagonal pattern can be obtained at higher voltages. Because the anodization of aluminum requires the rearrangement of the oxide layer, the evolution of the patterns is quite slow.[11] Compared to the anodization process, electropolishing is more rapid and initial defects in the patterns can quickly evolve into more order patterns.

Recently, a theory of the pattern formation during electropolishing of aluminum was proposed by Yuzhakov and collaborators.[12,18] They found that the aluminum anode can exhibit both highly regular and randomly packed nanoscale striped and hexagonal patterns in commercial electropolishing electrolyte. The nonuniform interface creates higher electric fields at the ''hills'' relative to the ''valleys.'' A higher electric field at the hills increases the dissolution rate, while a lower electric field at the valleys decreases the dissolution rate. The net effect is that the dissolution reaction flattens the interface. However, the perturbed electric field also increases the adsorption of any surfactant that might be present. The surfactant adsorbs preferentially onto the hills due to the larger electric field. The adsorbed surfactant blocks the reaction sites, thus decreasing the dissolution rate. The adsorbed surfactant destabilizes the interface by making the hills higher and the valleys deeper. For certain parameter regions, these two effects are balanced and stable patterns form (see Fig. 1).

In our present work, we study the effect of interfacial energy on the pattern formation during the electropolishing of aluminum. We extend the model of Yuzhakov *et al.*[12] by including the interfacial energy contribution to the total Gibbs free energy of the anodic reaction. The present work is essentially divided in three parts: a detailed explanation of the modeling procedure, a mathematic analysis of our model, and experimental results.

In Sec. II, we derive a modified evolution equation using a long-wavelength expansion of the interfacial kinematic equation and an equation for the surfactant coverage. In Sec. III, the linearized evolution equation reveals that the interfacial energy changes the instability criteria and decreases the maximum growth rate of unstable modes. Additionally, a weakly nonlinear analysis is performed to predict regions of stable striped and hexagonal patterns. Finally, a spectral method is employed to numerically solve the evolution equation, which yields qualitatively the same results that our weakly nonlinear analysis predicts. In Sec. IV, we present the experimental results, which further support our theoretical predictions that hexagonal and striped patterns can be obtained in the same sample.

II. EVOLUTION EQUATION

A. Mechanism of pattern formation with interfacial energy

The paper by Yuzhakov *et al.*[12] introduced the competitive mechanism between dissolution rate and surfactant adsorption rate. However, it did not include interfacial energy, which we will show has a significant effect on the results.

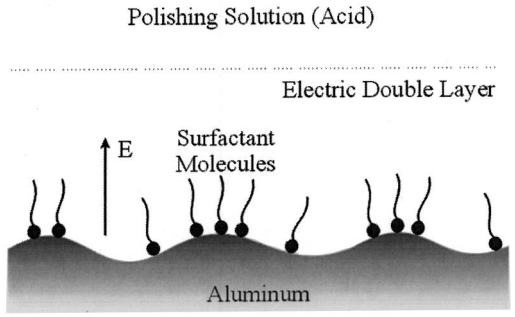

FIG. 1. Schematic of the mechanism of electropolishing in the presence of surfactants. Perturbations to the interface increase in the electric field on the ''hills'' relative to the ''valleys.'' The higher electric field at the hills increases the dissolution rate, but also increases the adsorption rate of surfactants. The interfacial energy inhibits the formation of areas with high surface curvature.

The interfacial energy adds additional stability to the interface by restraining areas of high surface curvature. This leads to stabilizing the short-wavelength disturbance and modifies the parameter region where stable patterns exist. Furthermore, we find that the interfacial energy is needed in the model in order to predict stable hexagonal patterns.

B. Effect of surface tension on dissolution rate

According to transition-state theory and electrode kinetics, the dissolution rate can be written as follows:[13]

$$K_r = K_r' \exp\left(\frac{-\overline{\Delta G_a^{\#}}}{RT}\right), \tag{1}$$

where K_r' represents the fieldless dissolution rate resulting from concentration and bulk mass transport, while $\Delta\overline{G_a^{\#}}$ denotes the electrochemical free energy of activation and can be separated, as will be showed in Eq. (2), into chemical and electrical components.[13] In the case of the deformation of a planar anode, the interfacial energy contributes to the total free energy. Therefore, we obtain $\Delta\overline{G_a^{\#}}$ as follows:

$$\Delta\overline{G_a^{\#}} = \Delta G_a^{\#} - (1-e)Z_0 F \Delta\psi_a + \frac{(1-e)\sigma(\nabla\cdot\mathbf{n})}{C_M}. \tag{2}$$

Here $\Delta G_a^{\#}$ is the chemical free energy of activation and is independent of the potential and e is the energy transfer coefficient, which can range from zero to unity.[13] For many reactions it is found to be extremely close to 0.5.[14] Z_0 is the charge on the ion, and $\Delta\psi_a$ is the anode potential difference across the double layer. The symbol σ denotes the interfacial energy, $\mathbf{n}$ is the unit outward normal vector, $\nabla\cdot\mathbf{n}$ is the mean interfacial curvature, and C_M represents the anode metal density. Combining Eqs. (1) and (2) gives

$$K_r = K_r^* \exp\left(\frac{\beta_r E}{k_B T} - \frac{(1-e)\sigma(\nabla\cdot\mathbf{n})}{C_M RT}\right). \tag{3}$$

Here $K_r^* = K_r' \exp(-\Delta G_a^{\#}/RT)$, β_r is a proportionality coefficient that is of the order of 10^{-31} J m V^{-1} for most metal anodes,[12,15] E is the anode electric field, and k_B is Boltzmann's constant.

C. Derivation of the evolution equation

We assume that the momentum and diffusion boundary layers are much larger than the electric double layer. Therefore, the velocity of the electrolyte solution and the concentration of dissolved ions are not considered in the analysis. We further assume that the electrolyte composition does not change such that the double-layer thickness and the anodic chemistry are not affected by changes in composition.

We use the Debye-Huckel approximation of the Poisson-Boltzmann equation to describe the potential field in the double layer:

$$\nabla^2\psi = \frac{2Z_0 F C_0}{\varepsilon}\sinh\left(\frac{Z_0 F\psi}{RT}\right) \cong \frac{\psi}{\delta_E^2}, \tag{4}$$

$$\psi|_{z\to\infty} = 0,$$

$$\psi_{z=h} = \psi_s,$$

where ψ_s is the potential at the anode relative to the bulk electrolyte and h is the deviation of the interface from a flat electrode. We solve Eq. (4) assuming that the potential is only dependent on the z direction. This gives the electric potential across the double layer for a flat interface.

$$\psi = \psi_s \exp\left(\frac{h-z}{\delta_E}\right). \tag{5}$$

The electric field in the double layer for a flat interface is found by taking the negative gradient of the electric potential:

$$E_0 = -\left.\frac{d\psi}{dz}\right|_{z=0} = \frac{\psi_s \exp(h/\delta_E)}{\delta_E} = \frac{\psi_0}{\delta_E}. \tag{6}$$

Here ψ_0 is the electric potential of a flat interface. It is found experimentally that the amplitude of the interfacial patterns is much smaller than the wavelength. From this, a long-wavelength expansion of Eq. (4) is used to derive the relationship between the anode interfacial electric field and the interfacial shape h:

$$E = -\left.\frac{\partial\psi}{\partial n}\right|_{z=h} \approx E_0 + E_1, \tag{7}$$

where $\partial/\partial n$ is the normal gradient and the deviation electric field $E_1 \ll E_0$ relative to the planar case is[12]

$$E_1 = -\frac{E_0}{2}[(\nabla h)^2 + \delta_E \nabla^2 h] \tag{8}$$

In order to demonstrate how the interfacial energy, the deviation field E_1, and the interfacial shape affect the dissolution rate, a long-wavelength expansion of the dissolution rate $K_r \approx K_r^0 + K_r^1$ is needed:

$$\frac{K_r^1}{K_r^0}=\frac{\beta_r}{k_BT}E_1-\frac{(1-e)\sigma\delta_E}{C_M\delta_E RT}\nabla^2 h+\frac{1}{2}\left(\frac{\beta_r}{RT}\right)^2 E_1^2 + \frac{1}{2}\left(\frac{(1-e)\sigma}{C_M\delta_E k_BT}\right)^2(\nabla^2 h)^2\delta_E^2. \tag{9}$$

Substituting Eq. (8) into Eq. (9) yields

$$\frac{K_r^1}{K_r^0}=-B_1(\boldsymbol{\nabla} h)^2-(B_1+B_2)\,\delta_E\nabla^2 h + \left(\frac{B_1B_1+B_2B_2}{2}\right)\delta_E^2(\nabla^2 h)^2, \tag{10}$$

where $B_1=\beta_r E_0/2k_BT$ and $B_2=(1-e)\sigma/C_M\delta_E RT$.

The parameter B_1 demonstrates the sensitivity of unshielded dissolution to field changes,[12] while B_2 represents the sensitivity of unshielded dissolution to interfacial energy changes. B_1 is a small dimensionless value for most dissolution reactions. For aluminum electropolishing, B_1 is in the range from 0.05 to 0.15 (Refs. 12 and 15) and B_2 is approximately in the range between 0.004 and 0.026 for reasonably values of σ (e.g., 30 mJ/m^2). Therefore, any terms that include B_1^2 and B_2^2 are ignored.

Yuzhakov *et al.*[12] introduced a short-wavelength cutoff mechanism to couple with the long-wavelength instability by using a quasisteady equation for the surfactant coverage:

$$D_s\nabla^2\theta+k_a-k_d\theta=0. \tag{11}$$

Upon expanding the surfactant coverage θ, the adsorption rate k_a, and the desorption rate k_d, we have

$$D_s^0\nabla^2\theta_1+k_a^1-k_d^0\theta_1=0. \tag{12}$$

The adsorption rate depends on the electric field and induced dipole moments of the surfactant.[16] Assuming the adsorption rate of the shielding molecule is dependent only on the difference of its polarizability relative to the others and the relative polarizability, we have

$$k_a=k_a^*\exp\left(\frac{\alpha E^2}{2k_BT}\right). \tag{13}$$

Here α is the difference in effective polarizability and can be obtained from the Debye-Langevin equation $\alpha=\alpha_0+P_0^2/3k_BT$, in which α_0 is the difference in polarizabilities and P_0 is the difference in permanent dipole moments.[12] Equation (13) is expanded about E_0 to obtain k_a^1 to $O(E_1^2)$:

$$k_a^1=\frac{\alpha E_0}{k_BT}k_a^0E_1+\frac{1}{2}\frac{\alpha}{k_BT}\left(\frac{\alpha E_0^2}{k_BT}+1\right)k_a^0E_1^2. \tag{14}$$

Substituting Eqs. (8) and (14) into Eq. (12) gives

$$\left(\frac{D_s^0}{k_d^0}\right)\nabla^2\theta_1-\theta_1=B_3\left[(\boldsymbol{\nabla} h)^2+\delta_E\nabla^2 h-\frac{\delta_E^2}{4}\left(\frac{\alpha E_0^2}{k_BT}+1\right)\times(\nabla^2 h)^2\right], \tag{15}$$

where the dimensionless number B_3 is a normalized activation energy that gives the sensitivity of the adsorption rate to field changes:

$$B_3=\frac{1}{2}\frac{k_a^0}{k_d^0}\frac{\alpha E_0^2}{k_BT}.$$

The kinematic condition at the interface is found by performing a mass balance:[12]

$$\frac{\partial h}{\partial t}=K_r^0\theta_1-K_r^1. \tag{16}$$

Combining the above equations yields the following evolution equation:

$$\frac{\partial h}{\partial t}-\left(\frac{D_s^0}{k_d^0}\right)\nabla^2\left(\frac{\partial h}{\partial t}\right)=k_r^0B_3\Bigg[-(1-\nu)\,\delta_E\nabla^2 h-(1-\nu)(\boldsymbol{\nabla} h)^2 - \delta_E\left(\frac{D_s^0}{k_d^0}\right)\nu\nabla^4 h-\left(\frac{D_s^0}{k_d^0}\right)\nu\nabla^2(\boldsymbol{\nabla} h)^2 + \frac{\delta_E^2}{4}\left(\frac{\alpha E_0^2}{k_BT}+1\right)(\nabla^2 h)^2+\nu'\,\delta_E\nabla^2 h - \left(\frac{D_s^0}{k_d^0}\right)\nu'\,\delta_E\nabla^4 h\Bigg], \tag{17}$$

where $\nu=B_1/B_3$ denotes the ratio of the activation energies for the dissolution and adsorption, while $\nu'=B_2/B_3$ represents the ratio of interfacial energy and activation energy for the adsorption. In order to make the governing equation dimensionless, we use the following scalings:

$$t=\frac{\nu(D_s^0/k_d^0)}{k_r^0B_3(1-\nu)^2\delta_E}\tau,$$

$$(x,y)=\left(\frac{\nu}{1-\nu}\right)^{1/2}\left(\frac{D_s^0}{k_d^0}\right)^{1/2}(X,Y),$$

$$h=\delta_E H.$$

After simplifying, we finally obtain the dimensionless evolution equation

$$H_\tau-s\nabla^2H_\tau=-(\boldsymbol{\nabla} H)^2-\left(1-\frac{p}{s}\right)\nabla^2H-(1+p)\nabla^4H - \nabla^2(\boldsymbol{\nabla} H)^2+2\xi(\nabla^2H)^2, \tag{18}$$

where

$$s=\frac{1-\nu}{\nu},\quad p=\frac{\nu'}{\nu}.$$

Here ξ represents the operating parameter that includes the coupling between electric field, adsorption, and interfacial energy:

$$\xi=\frac{\delta_E^2}{8\nu}\left(\frac{k_d^0}{D_s^0}\right)\left(\frac{\alpha E_0^2}{k_BT}+1\right)-\frac{\nu'B_2\delta_E^2k_d^0}{4\nu D_s^0}.$$

III. MATHEMATICAL ANALYSIS OF THE MODEL

A. Linear instability analysis

The value for ν remains close to 0.5 in the voltage range from 20 to 80 V.[12,18] We use the value of $\nu=\frac{16}{25}=0.64$ for the nonlinear analysis. Our linear stability analysis starts with linearizing Eq. (18):

$$\frac{\partial(H-s\nabla^2 H)}{\partial\tau}=-\left(1-\frac{p}{s}\right)\nabla^2 H-(1+p)\nabla^4 H. \quad (19)$$

Substituting a normal mode $H\sim\exp[\lambda\tau+i(kx+ly)]$ into Eq. (19) yields the growth rate

$$\lambda=\frac{\left(1-\frac{p}{s}\right)q^2-(1+p)q^4}{1+sq^2}, \quad (20)$$

where $q^2=k^2+l^2$. The values of the wave number that give positive growth rates are

$$q^2\leqslant\frac{\left(1-\frac{p}{s}\right)}{1+p}. \quad (21)$$

The maximum growth rate q_m is given by

$$q_m^2=\frac{-1+\sqrt{\frac{1+s}{1+p}}}{s}. \quad (22)$$

The case when the interfacial energy is not considered can be recovered easily by setting $p=0$. Notice that the addition of the interfacial energy decreases the value of the maximum growth rate and the region of unstable wave vectors.

B. Weakly nonlinear analysis

A weakly nonlinear analysis is performed on the evolution equation by expanding the height in terms of the unstable modes of the maximum growth rate, the first harmonic modes of the unstable modes, and the resonant modes. Higher-order modes are neglected. Figure 2 gives all the modes that contribute to the evolution of the height H.
The expansion of the height in terms of the various modes is given in Eq. (23) (Ref. 12):

$$H=\sum_{j=1}^{6}\left[W_j\exp(i\mathbf{k}_j\cdot\mathbf{r})+V_j\exp(2i\mathbf{k}_j\cdot\mathbf{r})+U_j\exp(i\mathbf{k}_{rj}\cdot\mathbf{r})\right]. \quad (23)$$

Here W_j represents unstable modes, V_j represents the stable harmonic modes, and U_j represents the stable resonant modes. We follow the standard procedure[19] by substituting Eq. (23) into the evolution equation (18) and take the inner product to get an ordinary differential equation for each unstable mode. An adiabatic reduction is performed where the dynamics and quadratic interactions of the stable modes are assumed negligible:

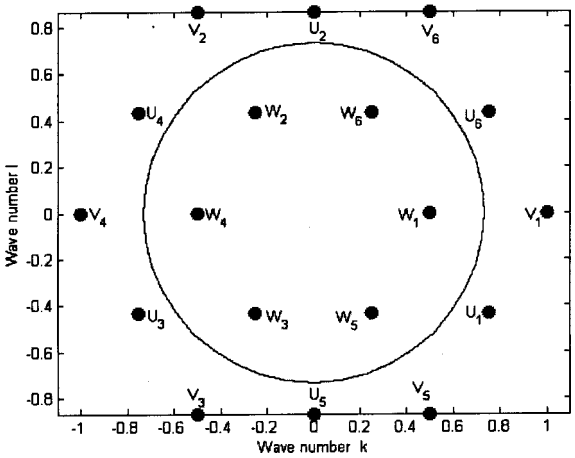

FIG. 2. Diagram of the unstable, stable, and resonant modes used in the weakly nonlinear analysis.

$$\frac{dW_1}{d\tau}=\gamma_0 W_1+\gamma_1 W_2^* W_3^*-\gamma_2|W_1|^2 W_1-\gamma_3(|W_2|^2+|W_3|^2)W_1,$$

$$\frac{dW_2}{d\tau}=\gamma_0 W_2+\gamma_1 W_3^* W_1^*-\gamma_2|W_2|^2 W_2-\gamma_3(|W_3|^2+|W_1|^2)W_2,$$

$$\frac{dW_3}{d\tau}=\gamma_0 W_3+\gamma_1 W_1^* W_2^*-\gamma_2|W_3|^2 W_3-\gamma_3(|W_1|^2+|W_2|^2)W_3. \quad (24)$$

If the interfacial energy is ignored, the coefficients of the amplitude equation are

$$\gamma_0=\frac{16}{81},$$

$$\gamma_1=\frac{16}{405}(16\xi-5),$$

$$\gamma_2=-\frac{16}{2835}(16\xi-5)(8\xi-7),$$

$$\gamma_3=-\frac{16}{1215}(16\xi-3)(16\xi-5).$$

Similarly, we obtain the amplitude equations for the case when the interfacial energy is not ignored. For convenience, we select $p=0.212$ such that $q_m=1/2$ and obtain the following values for the amplitude equation coefficients:

$$\gamma_0=\frac{400}{5329},$$

$$\gamma_1=\frac{4}{73}(4\xi-3),$$

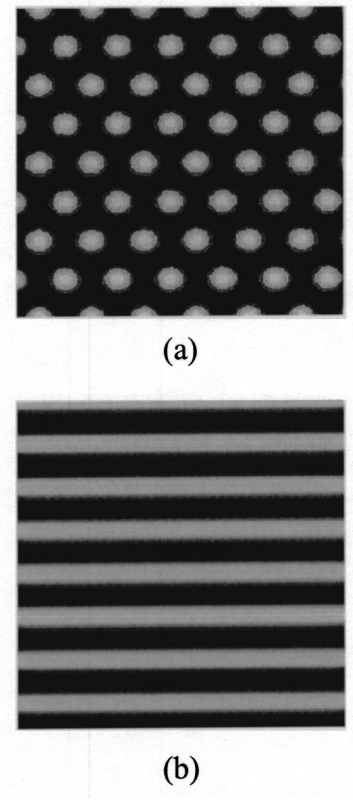

FIG. 3. Results from nonlinear simulation with interfacial energy included. $p=1071/5329$ and $s=9/16$. (a) Stable hexagonal patterns $\xi=0.2$ and (b) stable striped patterns $\xi=0.6$.

$$\gamma_2=-\frac{146}{2975}(4\xi-3)\xi,$$

$$\gamma_3=-\frac{73}{1375}(4\xi+1)(4\xi-3).$$

The results reveal that the interfacial energy does significantly affect the amplitude equation coefficients.

In Eq. (24), W_1, W_2, and W_3 are all complex modes that can be written as a product of the real and complex parts:

$$W_j=R_j\exp(i\varphi_j). \tag{25}$$

Here R_j is the real amplitude and φ_j represents the phase amplitude of the unstable modes. After substituting Eq. (25) into Eq. (24) and assuming that only the amplitude dynamics is important at long times,[12] we obtain

$$\frac{dR_1}{d\tau}=\gamma_0R_1+|\gamma_1|R_2R_3-\gamma_2|R_1|^2R_1-\gamma_3(|R_2|^2+|R_3|^2)R_1,$$

$$\frac{dR_2}{d\tau}=\gamma_0R_2+|\gamma_1|R_1R_3-\gamma_2|R_2|^2R_2-\gamma_3(|R_1|^2+|R_3|^2)R_2,$$

$$\frac{dR_3}{d\tau}=\gamma_0R_3+|\gamma_1|R_1R_2-\gamma_2|R_3|^2R_3-\gamma_3(|R_1|^2+|R_2|^2)R_3. \tag{26}$$

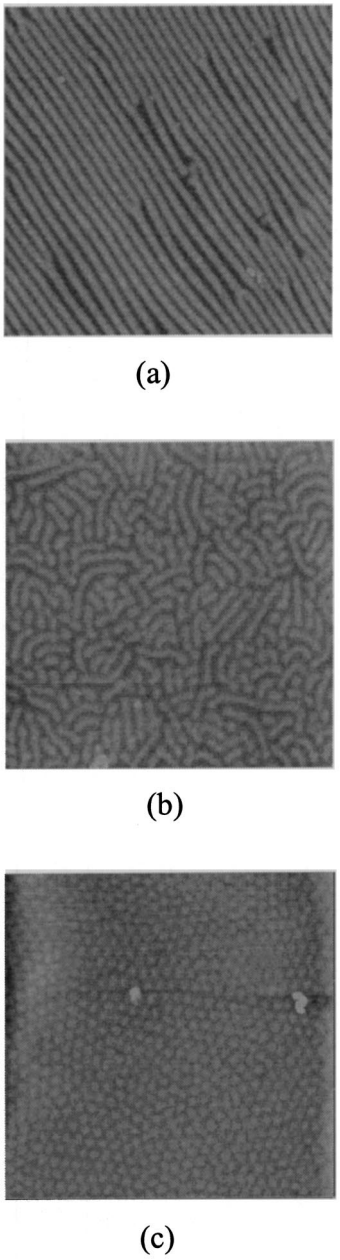

FIG. 4. AFM images showing different patterns that form on the same sample electropolished at 56 V for 30 s. (a) Striped pattern, (b) Random pattern, and (c) hexagonal pattern.

Consequently, four types of steady-state solutions are obtained: (1) striped patterns if $R_1=\sqrt{\gamma_0/\gamma_2}$ and $R_2=R_3=0$; (2) hexagonal patterns if $R_1=R_2=R_3$, where

$$R_1=\frac{|\gamma_1|+\sqrt{|\gamma_1|^2+4\gamma_0(\gamma_2+2\gamma_3)}}{2(\gamma_2+2\gamma_3)}; \tag{27}$$

(3) mixed patterns if two or three amplitudes are not zero; and (4) a flat interface if all of the amplitudes are zero. To determine the stability of the patterns, we calculate the eigenvalues of the Jacobian matrix of the amplitude equation.

TABLE I. Comparison of the values of ξ that give stable patterns and real amplitudes R_j (the interval of existence). The values for Yuzhakov *et al.* were found by using the coefficient equations given in Ref. 12.

	Reference 12	This work ($\sigma=0$)	This work ($\sigma=60$ mJ/m^2)
Hexagon existence	(0.53, 0.93)	(0.25, 0.31)	(−0.22, 0.75)
Stable hexagon	(0.53, 0.88)	Never stable	(−0.15, 0.30)
Stripe existence	(0.31, 0.88)	(0.31, 0.88)	(0.00, 0.75)
Stable stripe	(0.84, 0.88)	Never Stable	(0.00, 0.75)

C. Numerical simulation

To help verify our calculations, we perform a full nonlinear numerical simulation of the evolution equation (18). The height H was expanded in terms of Fourier modes in the x and y directions:[17]

$$H=\sum_{n=-N_1/2}^{N_1/2-1}\sum_{m=-N_2/2}^{N_2/2-1} W_{nm}(t)\exp[i(nx+my)]. \quad (28)$$

Here n and m represent the wave number of the x and y modes, respectively. Upon substituting Eq. (28) into Eq. (18), multiplying by $\exp[-i(nx+my)]$, and integrating, we get $N_1\times N_2$ ordinary differential equations for the amplitudes of each Fourier mode. The set of differential equations was integrated using a split fourth- and fifth-order Runga-Kutta method until a steady state is reached. A plot of the steady-state solutions for different values of p and ξ is given in Fig. 3.

IV. EXPERIMENTS

Alfa AESAR, Puratronic 99.998%, polycrystalline Al foil, 0.5 mm thick, was used as the anode. A 304 stainless-steel cathode was placed parallel to the anode 3 mm away. We used a Kenwood PDS 120-6 programmable power supply to electropolish the Al samples without agitating the electrolyte. To avoid excessive increases in the anode temperature, we electropolished the samples using six pulses of 5 s in duration. The voltage was turned off after 5 s until the anode temperature steadied at 15 °C.

The 0.8-cm^2 Al samples are first immersed in 5% sodium hydroxide solution for 30 s at 60 °C, rinsed in de-ionized water, washed in 35% nitric acid solution at room temperature for 5–10 s, rinsed in de-ionized water again, and then electropolished for 30 s (six pulses) in the electrolyte. The electrolyte consisted of 70 vol. % ethanol, 10 vol. % 2-butoxyethanol, 13.8 vol. % de-ionized water, and 6.2 vol. % perchloric acid. After the electropolishing procedure, the Al surfaces were imaged with an atomic force microscope (AFM).

Our model predicts that higher values of ξ give striped patterns, while lower values of ξ produce hexagonal patterns, which was demonstrated experimentally by Yuzhakov *et al.*[12,18] We find experimentally that the hexagonal and striped patterns can coexist on the same sample (Fig. 4), which is in agreement with our model predictions. Similarly, Konovalov *et al.*[10] found that there are different topographies on different crystalline grains of the same polycrystalline Al surface, in which stripes were observed for only 10%–20% of the grains of a sample. Using Al single crystals in their experiment eliminated this uncertainty related to the grain distribution.

V. DISCUSSION

Table I compares the pattern stability and the interval of existence of three different sets of amplitude coefficients: (1) the coefficients of Ref. 12, (2) our coefficients with $\sigma=0$ mJ/m^2, and (3) our coefficients with $\sigma=60$ mJ/m^2. We find both the interval of existence, such that R_j is real, and the values of ξ, which give all negative eigenvalues. Our stability analysis using the coefficients from Yuzhakov *et al.*[12] shows that hexagonal solutions can exist for $\xi\in(0.53,0.93)$, which is in agreement with their results. This analysis also shows that stripes can exist for $\xi\in(0.31,0.88)$, which is consistent with the published values. However, the stable region $\xi\in(0.84,0.88)$ for stripes is inconsistent with their published values $\xi\in(0.68,0.88)$, while the result for stable hexagons is consistent with the published values. The analysis from our coefficients (without the interfacial energy) shows that neither hexagons nor stripes are stable within the interval of existence. When a nonzero interfacial energy is included, the analysis gives the interval of existence for the hexagons $\xi\in(-0.22,0.75)$, while stripes exist in the range of $\xi\in(0,0.75)$. Stability analysis predicts that stripes are always stable for $\xi\in(0,0.75)$, while hexagons are always stable for $\xi\in(-0.15,0.30)$. It is emphasized here that stable hexagons and stripes can coexist in the range of $\xi\in(0,0.30)$, which was shown in our experiments. We therefore conclude that the interfacial energy is needed in this case to predict stable patterns.

A nonlinear simulation of the evolution equation (18) was performed to help verify the weakly nonlinear analysis. The simulation showed that when values of p, s, and ξ are used such that the weakly nonlinear analysis predicts stable stripes, the numerical solution also gives stable stripes. The same is also true for hexagonal patterns. The simulation was also run using different initial conditions for values of ξ where both stable stripes and hexagons are predicted. Here we find that the final stable pattern is determined by the initial conditions of the simulation. Initial conditions that were close to stripes gave striped patterns, and initial conditions that were closer to hexagons gave stable hexagonal patterns.

Plots of the numerical simulation for values of $p=1071/5329$, $s=9/16$, and $\xi=0.2$ and 0.6 are given in Fig. 3. For $\xi=0.2$ stable hexagons were found, while striped patterns are formed when $\xi=0.6$. We conclude that the numeri-

cal simulation yields the same results as the weakly nonlinear analysis.

We theoretically and experimentally showed that hexagons and stripes could be observed on the same sample. As existing experimental results have revealed, we found that striped patterns appear at lower voltages, while hexagonal patterns can only be observed at higher voltages. Static solutions of hexagons and stripes and stability analysis show that hexagons are always stable in the range of $\xi \in (-0.15,0)$ and then comes the existence of stripes when $\xi \in (0,0.75)$. When $\xi \in (0,0.30)$, both hexagons and stripes are stable until ξ exceeds 0.30, which leads to unstable hexagons and stable stripes. Csahok and Misbah[20] have shown that the separation of hexagonal and striped fronts can only occur when the control parameter is increased to a certain value. We remind the reader that the parameter ξ is inversely proportional to the control parameter, the voltage.

It has been found[21] that hexagons appear through a subcritical bifurcation, while stripes are created via a supercritical bifurcation when the amplitude coefficients are real and reflection symmetry exists in the amplitude equations. In our weakly nonlinear analysis, the amplitude equations (26) have reflection symmetry. This may be the reason why we always see hexagonal patterns first and stripes later when the control parameter is increased. However, the coefficients γ_1, γ_2, and γ_3 are simultaneously dependent on the control parameter, the voltage. We should emphasize that because the coefficients are simultaneously dependent on the control parameter, our plot of amplitude against control parameter is different from the traditional bifurcation diagram (e.g., pitchfork bifurcation).[22]

VI. CONCLUSION

We have modified the existing theory by including the effect of interfacial energy. The analysis shows that the modified model is able to predict stable striped and hexagonal patterns that are seen in the experiments. A linear instability analysis was performed and shows that interfacial energy changes the linear stability criteria by making the region of unstable wave vectors smaller and reducing the maximum growth rate. The weakly nonlinear analysis showed that the interfacial energy significantly alters the parameter regions where stable striped and hexagonal patterns can exist. In particular, we find that the interfacial energy needs to be included in the model in order to predict stable patterns. A numerical simulation of the evolution equation also predicts the stability and existence of stable striped and hexagonal patterns. Our experimental results are also in agreement with our model predictions.

We note here that the interfacial properties in our model are assumed isotropic. However, all experiments to date have used polycrystalline or crystalline aluminum.

The crystalline structure would give rise to anisotropic properties and would significantly change the evolution equation and resulting patterns. Our future work will focus on introducing anisotropy into the model through interfacial energy and surface diffusion.

ACKNOWLEDGMENTS

This work was supported by a grant from the National Science Foundation (No. CTS-0084425). We thank Professor Hsueh-Chia Chang and Dr. Vadim V. Yuzhakov for helpful discussions.

*Author to whom correspondence should be addressed. Electronic address: djohnson@coe.eng.ua.edu

[1] Research Group for Functionalizing of Aluminum and its Surface Films, Light Metal Education (unpublished).
[2] D. Al-Mawlawi, N. Coombs, and M. Moskovits, J. Appl. Phys. **70**, 4421 (1991).
[3] D. Crouse, Y. H. Lo, and A. E. Miller, Appl. Phys. Lett. **76**, 49 (2000).
[4] H. Masuda, H. Yamada, and M. Satoh, Appl. Phys. Lett. **1**, 2770 (1997).
[5] F. Li, L. Zhang, and R. M. Metzger, Chem. Mater. **10**, 2470 (1998).
[6] G. E. Thompson and G. C. Wood, in *Anodic Films on Aluminum*, edited by J. C. Scully (Academic, New York, 1983).
[7] R. E. Ricker, A. E. Miller, and D. F. Yue, J. Electron. Mater. **25**, 1585 (1996).
[8] S. Bandyopadhyay, A. E. Miller, H. C. Chang, G. Banerjee, V. V. Yuzhakov, D. F. Yue, R. E. Ricker, S. Jones, J. A. Eastman, E. Baugher, and M. Chandrasekhar, Nanotechnology **7**, 360 (1996).
[9] D. Landolt, Electrochem. Acta **1**, 32 (1987).
[10] V. V. Konovalov, G. Zangari, and R. M. Metzger, Chem. Mater. **8**, 1949 (1999).
[11] D. Crouse, Y. H. Lo, and A. E. Miller, Appl. Phys. Lett. **76**, 49 (2000).
[12] V. V. Yuzhakov, H. C. Chang, and A. E. Miller, Phys. Rev. B **56**, 12 608 (1997).
[13] A. J. Bard and L. R. Faulkner, *Electrochemical Methods* (Wiley, New York, 1980).
[14] V. G. Levich, *Physicochemical Hydrodynamics* (Prentice-Hall, Englewood Cliffs, NJ, 1962).
[15] D. A. Jones, *Principles and Prevention of Corrosion* (Prentice-Hall, Upper Saddle River, NJ, 1996).
[16] J. N. Israelachvili, *Intermolecular and Surface Forces* (Academic, London, 1985).
[17] C. Canuto, M. Y. Hussaini, A. Quarteroni, and T. Zang, *Spectral Methods in Fluid Dynamics* (Springer-Verlag, Berlin, 1988).
[18] V. V. Yuzhakov, P. V. Takhistov, A. E. Miller, and H. C. Chang, Chaos **9**, 62 (1999).
[19] P. Manneville, *Dissipative Structures and Weak Turbulence* (Academic, Boston, 1990).
[20] Z. Csahok and C. Misbah, Europhys. Lett. **47**, 331 (1999).
[21] G. H. Gunaratne, Q. Ouyang, and H. L. Swinney, Phys. Rev. E **50**, 2802 (1994).
[22] M. Golubitsky and D. G. Schaeffer, *Singularities and Groups in Bifurcation Theory* (Springer-Verlag, New York, 1985), Vol. I.